TASK QUARTERLY 6 No 1 (2002), 79–100

HYDRAULIC DEVELOPMENT OF A CENTRIFUGAL PUMP IMPELLER USING THE AGILE TURBOMACHINERY DESIGN SYSTEM

KRZYSZTOF DENUS[1] AND COLIN OSBORNE[2]

[1] *CTD Technology – Ing. Buro Denus,*
Stationstraße 37, Postfach 12, CH-8487 Zell, Switzerland
denus@ctd-tech.ch

[2] *Concepts NREC,*
217 Billing Farm Rd., White River Jct., VT 05001, USA
cosborne@conceptseti.com

(Received 15 August 2001; revised manuscript received 28 December 2001)

Abstract: The impeller of an existing industrial pump (with both geometry and performance known) was analyzed and redesigned using an integrated, design/analysis, turbomachinery geometry modeling and flow simulation system. The purpose of the redesign was to achieve improved impeller performance (at the duty point). Fluid dynamics and geometry modeling parts of the design/analysis system were systematically applied: a) to analyse the existing impeller (impeller A), which was designed using conventional (routine in industry) hydraulic layout procedures, and b) to develop a new impeller (impeller B), using a coupled, multilevel 1D-Q3D-3D for the design and optimization. This paper discusses the features and advantages of the integrated design system, in which the coupled CAD/CFD approach is fully implemented. The analysis results are presented for impellers A and B, with the latter demonstrating a predicted increased efficiency and smaller size. Comparisons of the CFD results for both impellers reveal internal flow features that explain the improved impeller B performance levels.

Keywords: impeller design, CFD analysis, turbomachinery design optimization, internal flow analysis

Notation

B – impeller channel width;

BEP – best efficiency point;

Beta – blade angle;

E – impeller flow modeling parameter – the ratio between the secondary zone area and the total area at the impeller outlet;

H – developed head (pressure rise);

L_{ax} – axial length of the impeller channel;

LE – impeller blade leading edge;

M – meridional distance;
Q – flow rate;
R – radius, impeller contour coordinate in the radial direction;
$S3_x$ – local coordinate in the pitchwise direction;
$S3_y$ – local coordinates in the spanwise direction;
TE – impeller blade trailing edge;
Z – impeller contour coordinate in the axial direction.

1. Introduction

This paper discusses and presents the results of the application of the Agile Engineering Design System® [1], for the analysis and redesign of an exisiting industrial pump impeller. The subject impeller of this paper is from a high specific speed centifugal pump stage which was designed by Sulzer Pumps Company, and was later the subject of a research program at the Swiss Federal Institute of Technology in Zurich. The data which support the work described herein were derived from [2] and were used to reconstruct the key blading features of the tested impeller. In this paper, this digitally reconstructed baseline impeller is referred to as impeller A. The new impeller, whose geometry was generated by the application of the Agile system, is referred to as impeller B, which could serve as a replacement for impeller A.

Within the redesign process, two steps were undertaken in order to improve the baseline pump impeller A:

1. To analyze the performance of the baseline impeller A using the multilevel analysis tools available within the Agile system, which includes 1D, Q3D, and fully 3D, Navier-Stokes solvers.
2. To redesign impeller A to yield higher efficiency, using the same Agile tools, in particular its 3D geometry definition and CFD performance prediction codes.

The results presented in this paper are limited to the BEP operation, at which impeller A was analyzed, and for which impeller B was developed. However, for both impellers, flow calculations were conducted at the part load operation, but these will be reported separately. Future work on this case will include the instability analysis. No attempt was made at this point to include the instability effects in this analysis due to the lack of information available in the public domain for the pump A spiral volute geometry. Detailed investigations at part load operation will require coupled impeller-volute CFD computations.

2. The Agile Engineering Design System

An overview of the Agile Engineering Design System, adopted from [1], is shown in Figure 1. The underlying concept of the Agile system is that it consists in the computer implementation of the design and analysis tools which:

- organize and execute the integrated and automated multilevel (1D-Q3D-3D) approach, and
- allow their use either in the structured way, as shown in Figure 1 (*i.e.*, from the 1D, through the Q3D to the fully 3D design and analysis), or permit their use in a more flexible fashion (*i.e.*, allowing the user, at each phase of the design

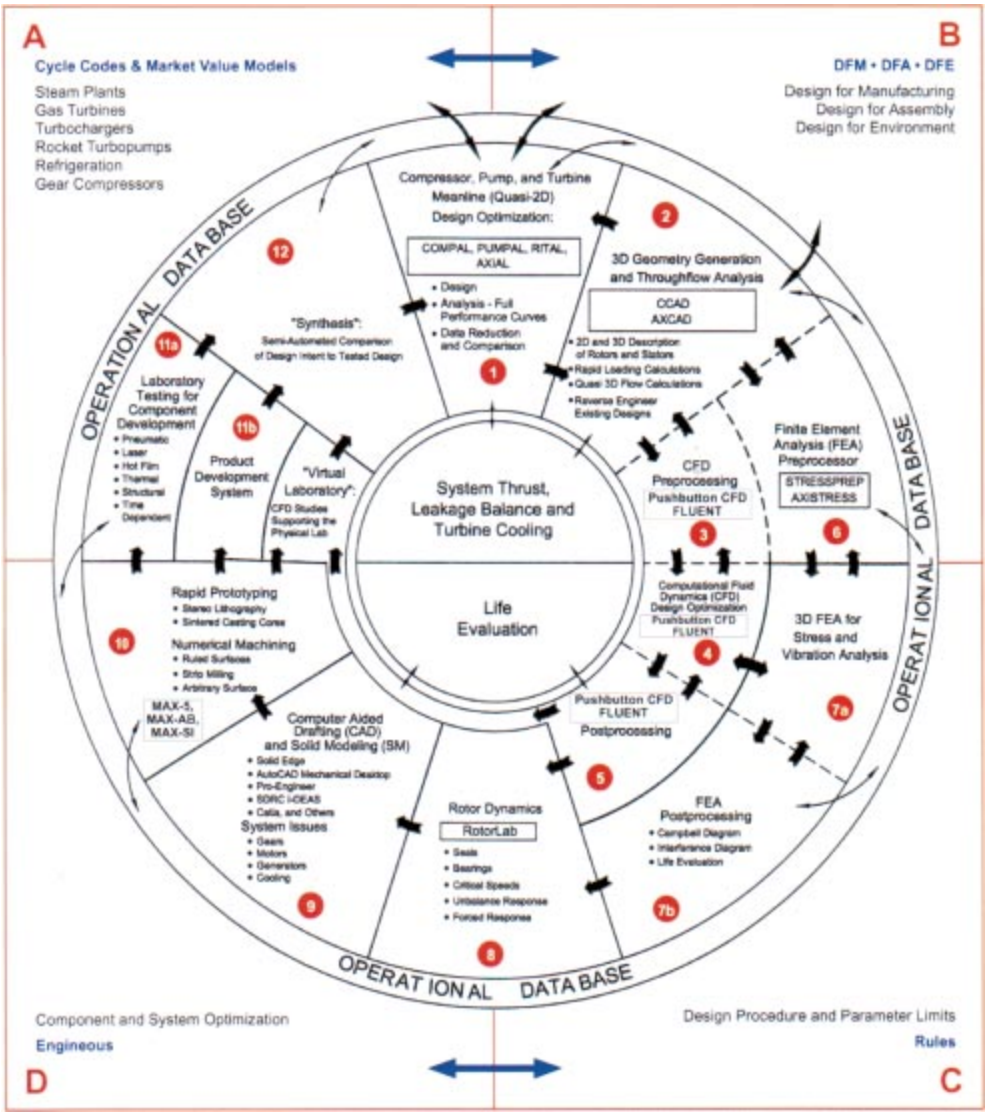

Figure 1. The structure of the Agile Engineering Design System

cycle, to make use of appropriate tools for the design tasks and for the stage specifications). In this manner, different combinations of the design and analysis codes can be applied for the design task, depending on the design specifications and the pursued design goals.

Different codes, whose features and interoperability are mentioned later, are equipped with interactive Graphical User Interfaces, and are tightly integrated and designed to work in a bi-directional way. The purpose is to ensure that data derived at one design level are made immediately available for use at another (either higher, or lower) design level, as shown in Figure 1. The transfer of data between the codes

representing different design levels is made fully automatic. Another important feature is to store both the design solutions and the results of their flow analyses, including all geometric and performance parameters at all levels, in order to efficiently conduct comparative parametric studies. These facilities allow the generation and screening of design candidates, either manually (*i.e.*, by the designer) or automatically (*i.e.*, via AI-based systems like iSight™) in the process of searching for the optimum design solution which satisfies the design goals and restrictions.

The principle of working with the Agile system in a structured way, as given by the inner path arrows in Figure 1, can be explained as follows. The first level analysis or design calculation is performed by the meanline code. The input and output parameters are limited to the global performance data, such as flow rate and total developed head, and include geometric and fluid dynamic parameters at design stations along the flowpath. The design stations are located at the inlet and outlet edges of bladed components, or at the inlet and outlet of vaneless components. The calculation process includes all components which define the pump stage. If the machine is a multistage unit, all stages are included in the calculation. There are three possible modes in the meanline code.

1. The analysis mode – in this case the performance (*e.g.*, head rise and efficiency) is to be predicted for a given geometry (where the data are limited to each component's inlet and outlet stations) and flow rate(s).
2. The design mode – in which certain geometric and flow design parameters are prescribed and the code defines the inlet and outlet geometry of each component in order to achieve the required (design) head at a given (design) flow rate.
3. The data reduction mode – in which the exisiting machine geometry, its overall tested performance curves, and measured data (particularly static pressures) at selected interstage locations are input. The code derives component and stage performance and design parameters, which can be used as the reference base for future stage optimization work.

The purpose of the meanline code is to compute the velocity triangles at critical stations along the stage flow path. The flow kinematic parameters thus derived allow the establishment of diffusion levels and loss coefficients in each component, and the design parameters for first-order design criteria. More details on the 1D procedures implemented in the meanline code are given in [1], [3], and [4].

Having defined or analysed the components at their inlet and outlet stations, the derived design data are readily available for transfer to three-dimensional codes for the geometry definition and flow analysis. Both simplified rapid loading techniques and conventional Q3D inviscid flow analysis methods are available for fast blading shape optimization, prior to the detailed viscous flow analysis using Navier-Stokes solvers. The rapid loading method is a simplified Q3D approach in which the impeller passage is modeled as a single streamtube. Despite its simplicity, the results of this modeling are very close to those of classical Q3D methods for most cases. The advantage of the rapid loading method is that it is directly coupled with the 3D geometry modeler, so that the fluid dynamic response is calculated instantenously (within milliseconds). Likewise, conventional Q3D analyses can be computed in a few seconds.

In geometrical terms, conventional blade modifications and working with advanced blade shape features are possible in the 3D, whose geometry definition code is directly coupled with the rapid loading program. Its advantage is that while working in real time it gives, within milliseconds, the fluid dynamic response to any change being interactively done on the component geometry.

Second-order design criteria are applied here in order to guide the optimization process towards the desired solution, including the blade loading criteria. More details on the procedures implemented at this level of the flow analysis are given in [5] and [6].

Subsequently, the most promising design candidates can be transferred to the next level of analysis, which includes the global performance prediction (*i.e.*, CFD-based performance curve generation), as well as the detailed internal flow structure studies. The CFD analysis process, starting with the model build-up, meshing of the computational domain, boundary and initial conditions specification, as well as the solver parameters settings, has been made fully automatic. Using defaults and preceding analyses results, the grid generation and the CFD computation can be performed without user intervention. The parameters used have been optimized to meet required accuracy in a short lapse time, so that a range of design alternatives can be generated and screened while reducing the design cycle. Based on the analysis and performance prediction results, the designer may proceed with additional evaluations available within the framework of the Agile system; these include:

- the stress (and thermal) analysis of the bladed components,
- the rotodynamic analysis of the rotor assembly,
- the build-up of the mechanical design CAD systems such as Pro/E, UG, Catia, *etc.*, and
- component manufacturing and testing.

Within the Agile system, it is possible to return to the previous step and attempt to redesign the components to achieve the design goals and to perform appropriate design iterations. An important element of the Agile system approach is the inclusion of data reduction techniques, which allows a feed-back system for refining and improving one dimensional modeling.

An example of the Agile system application for the analysis and redesign of an industrial pump impeller is presented in the next sections.

3. Baseline impeller geometry: 1D- and 3D-design models

Duty point parameters of the research pump under consideration are: flow rate, $Q = 0.196\,\mathrm{m}^3/\mathrm{s}$; head, $H = 5.8\,\mathrm{m}$; rotational speed $= 750\,\mathrm{rpm}$.

The baseline impeller geometry was derived from the data and the impeller pattern maker drawings published in [1]. These data were used to create:

- the one dimensional model for impeller A
- the three-dimensional digital model for impeller A.

The basic data which define the 1D model are given in Table 1. The baseline impeller shown with the pattern maker blade sections created in the 3D digital model is presented in Figure 2. The three-dimensional image of the digital model of impeller A is displayed in Figure 3.

Table 1. 1D models for impellers A and B

Parameter	Units	Impeller A Inlet	Impeller A Outlet	Impeller B Inlet	Impeller B Outlet
R, at the shroud	mm	135	162	128	161.5
R, at the hub	mm	43.3	162	43.3	148.5
Beta, at the shroud	deg	20	27	25	36
Beta, at the hub	deg	60	33	50	36
B, imp. width	mm	—	87	—	74
L_{ax}, imp. axial length	mm	—	167	0	159
LE inclination angle	deg	45	—	54.5	—
TE inclination angle	deg	—	90	—	80
Blade number	—	7	7	6	6

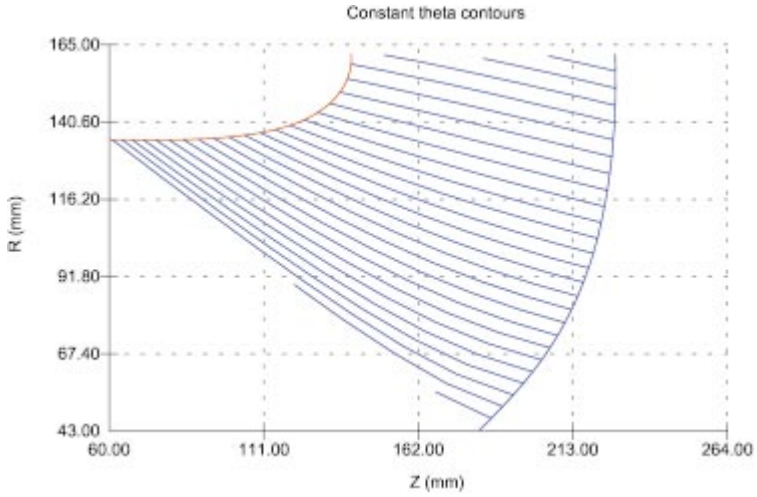

Figure 2. Impeller A: meridional profile showing blade cross-sections

Assumptions were made on the blade thicknesses, which were estimated to be 2mm at the LE and TE, and 5mm and 6mm along the shroud and hub sections, respectively. The hub and shroud blade contours and the blade angle distributions were derived from the pattern makers drawings and are presented in Figure 4 and Figure 5, respectively. These digitized data were used to create the 3D model of the impeller A in the three-dimensional impeller geometry modeler, CCAD [7].

4. One-dimensional analysis of impeller A

The set-up of the 1D model for impeller A analysis consisted of two parts:

1. geometrical modeling, and
2. fluid dynamics modeling.

Geometrical modeling required the input of the Table 1 data into the one-dimensional code, PUMPAL [8], which was run in the analysis mode in order to generate the LE and TE velocity triangles, loss levels and impeller and stage efficiency predictions. Fluid dynamic modeling consisted of selecting design parameter levels for:

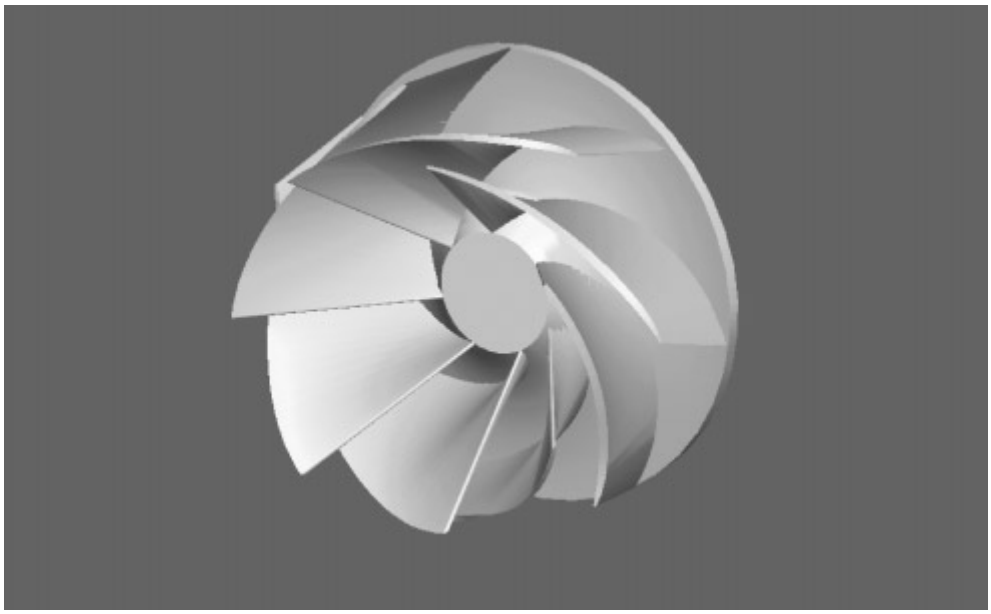

Figure 3. Impeller A: 3D digital impeller model

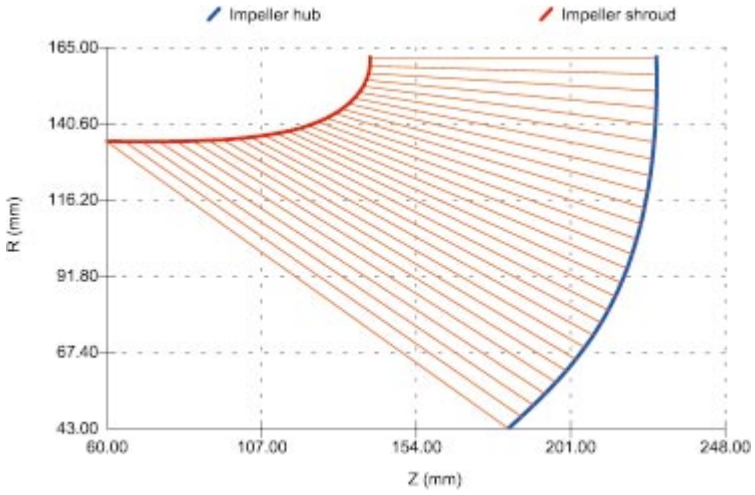

Figure 4. Meridional profile of impeller A with meshing for Q3D analysis

- blade and aerodynamic blockage,
- inlet meridional velocity ratio (shroud to RMS),
- inlet loss coefficient,
- impeller tip-model/jet-wake characteristics,
- impeller slip (or deviation) model,
- recirculation power level, and
- impeller diffusion: TEIS (Two Elements-in-Series),

with the empirical values of relevant parameters selected based on previous experience in the design and analysis of impellers of this specific speed. Details of the design

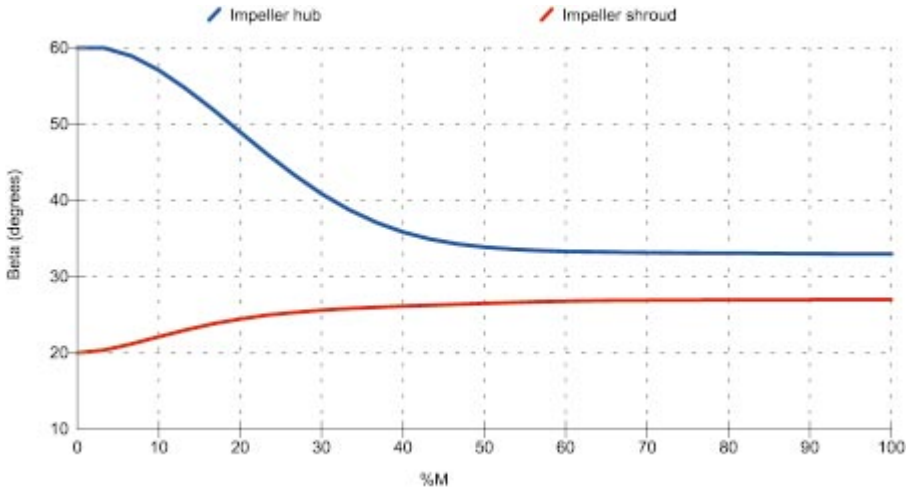

Figure 5. Blade angles distributions along hub and shroud for impeller A

analysis methods implemented in the one-dimensional code applied at this modeling level are given in [1].

Table 2 summarises the main output parameters resulting from the 1D design analysis. These results indicate large incidence angles along the impeller leading edge, and the existence of a considerable portion of the impeller discharge area which is occupied by low energy flow (wake region). These two characteristics alone contribute to the low (0.83) rotor efficiency predicted by the one-dimensional code, as given in Table 2. For both cases 1D models include the complete pump stage (*i.e.*, both impeller plus volute).

Table 2. 1D Analysis results for impellers A and B at BEP

Parameter	Units	Impeller A Inlet	Impeller A Outlet	Impeller B Inlet	Impeller B Outlet
Flow departure at the tip	deg	1.69 (inc.)	—	2.64 (inc.)	—
Flow departure at the RMS	deg	14.4 (inc.)	13.0 (dev. angle)	3.39 (inc.)	13.64 (dev. angle)
Flow departure at the hub	deg	26.5 (inc.)	—	4.85 (inc.)	—
E (sec. zone / total area)	—	—	0.426	—	0.28
Slip Factor (US definition)	—	—	0.731	—	0.76
Internal impeller loss	—	—	0.077	—	0.073
Impeller exit mixing loss	—	—	0.055	—	0.04
Rotor T-T efficiency	—	—	0.83	—	0.87
Stage T-T efficiency	—	—	0.79	—	0.82
Total Developed Head	m	—	5.8	—	5.8

Figure 6 shows the predicted (1D) Q-H performance curve for pump A, while Figure 7 presents the measured Q-H performance curve. By comparing Figure 6 and Figure 7, it can be seen that the predicted curve is quite accurate for head rise at the BEP, and for estimating the instability limit.

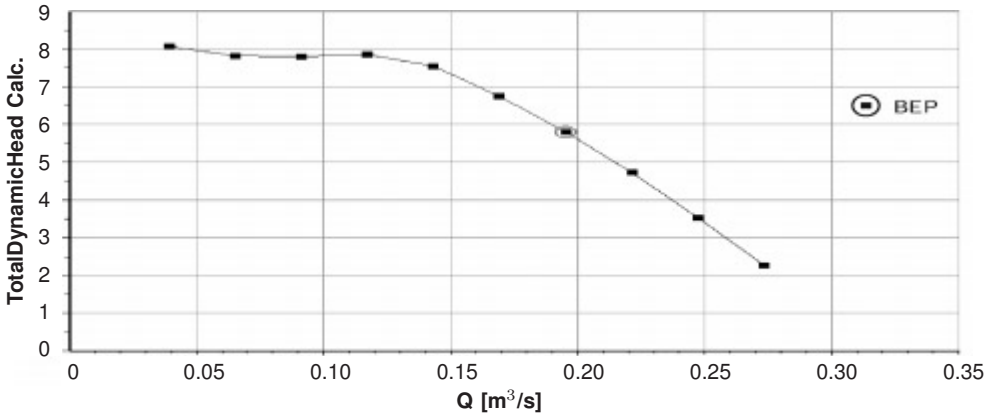

Figure 6. Pump A 1D meanline performance prediction

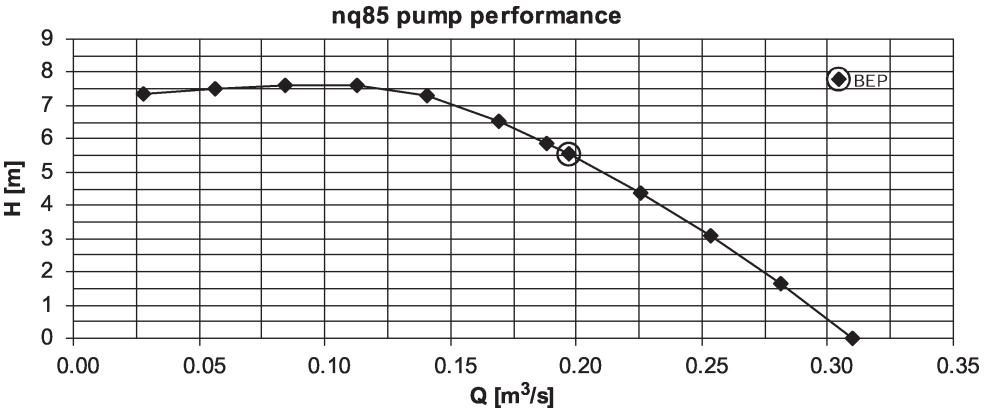

Figure 7. Pump A measured performance curve

5. Impeller A – 3D geometry model and Q3D flow analyses

The 3D impeller geometric model was created in the CCAD code by inputting the number of blades, the definition of the hub and shroud contours, and the associated hub and shroud blade normal thickness and wrap angle distributions. Appropriate curve fitting procedures (in CCAD) were employed to represent the hub and shroud contours and thickness distributions and to deduce the hub and shroud blade angle distributions.

Geometry and fluid dynamics features available in CCAD were used to analyze impeller A properties, such as the meridional channel and the blade passage areas, as well as blade loading. Q3D inviscid flow analysis was performed to derive information on blade loading for the existing impeller. Figure 8 shows the blade and flow angles along the hub and shroud contours, the differences between the two at the leading edge and the trailing edge giving the flow incidence and deviation angles, respectively. They agree well with the 1D analysis results, given in the Table 1, and they confirm the large hub inlet incidence angle.

Blade loading distributions, based on the velocity difference between the blade pressure and suction side at each computing station, are presented in Figure 9. The high incidence angle at the hub impeller inlet is reflected by the high blade loading

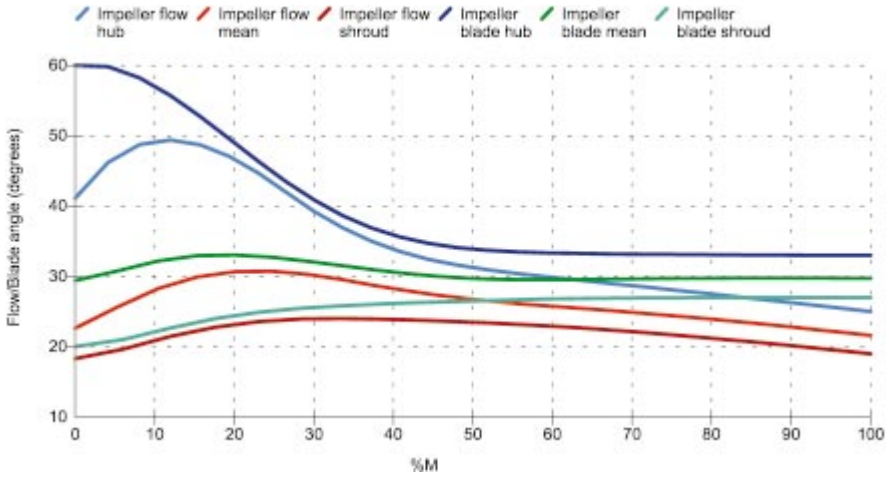

Figure 8. Flow and blade angles distributions along three blade

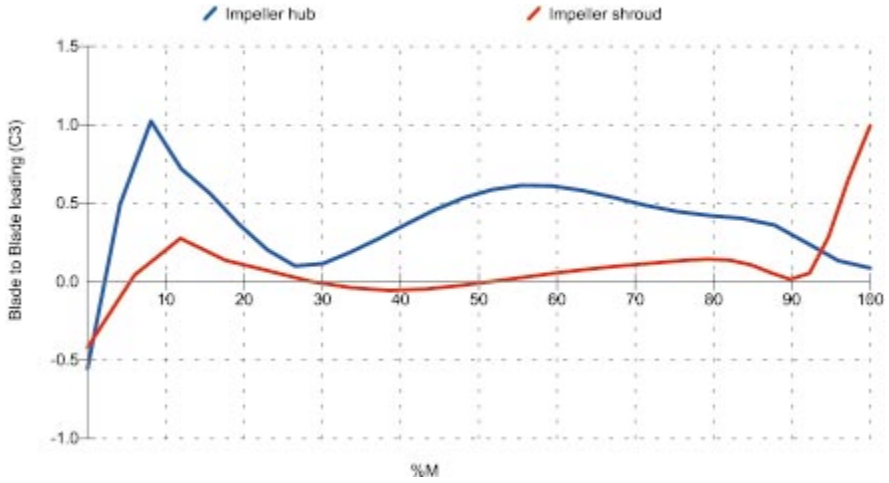

Figure 9. Impeller A blade loading predicted from simplified Q3D procedure

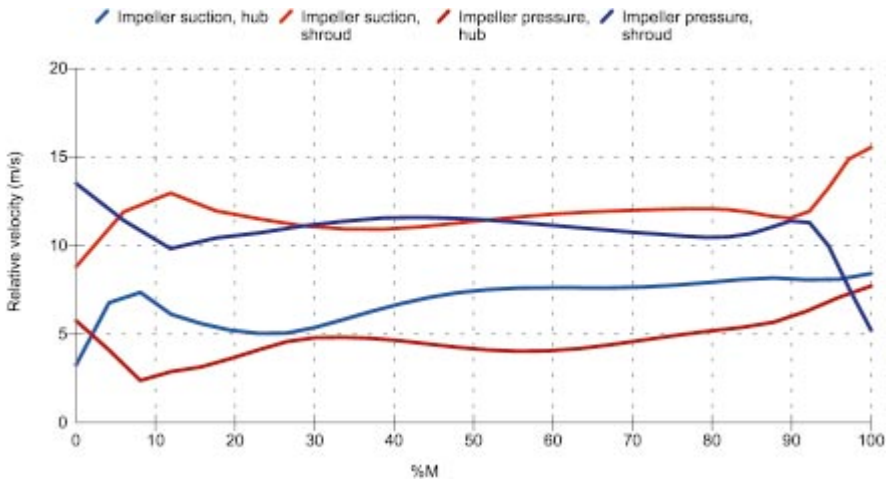

Figure 10. Impeller A relative velocities distributions from simplified Q3D procedure

downstream of the leading edge. The distribution of the blade loading in the rear 60% of the blade is mostly uniform and remains below the 0.6 blade loading level limit. The peak of the blade loading in the shroud / TE region results from the prohibitive curvature of the shroud contour (see Figure 4) for this Q3D computation. Figure 10 displays the relative velocity distributions along the hub and shroud contours with the effect of the high shroud curvature near the impeller exit clearly indicated.

6. Background and procedures for 3D viscous flow evaluations

Three-dimensional CFD analysis and global performance predictions were carried out using the Pushbutton CFD Navier-Stokes solver. Pushbutton CFD is an improved incompressible flow version of Prof. William Dawes' BTOB3D code. Within CCAD, Pushbutton CFD reads in the impeller geometry and completes the CFD analysis. The extension of the flow region upstream of the impeller is made automatically, while the extension downstream of the impeller was added as a vaneless diffuser element. Examples of the computational domain and gridding are displayed in Figures 11 and 12 (corresponding with impeller A).

The entire CFD model set-up and solver execution is completed automatically, consisting of the following steps.

A. Grid Generator

Pushbutton CFD creates a structured, single-block, contour-fitted H-type of grid. A standard topology has been established to ensure fast convergence time and an adequate solution accuracy for design iterations. These are the two key factors for the efficient application of the Navier-Stokes solvers in turbomachinery design cycles [9, 10]. The grid topology, consisting of 21 grid points in both the spanwise and pitchwise directions, and 71 grid points in the streamwise direction, was used for the analyses of impellers A and B. The user can modify the grid topology by changing the number of grid points as well as their density in any direction, for any component. Finer grids were employed throughout the calculation domain for analyses conducted at part load (below $0.7Q/Q_{BEP}$). The typical grid topology, based on the standard settings relevant to this study, is illustrated Figures 11 and 12.

B. Solver

The CFD solution is based on the three-dimensional, Reynolds-averaged Navier-Stokes equations, with appropriate pre-conditioning to handle incompressible flow. Finite volume formulation is used in the blade-relative frame using cylindrical coordinates. Mixing length turbulence model according to Baldwin-Lomax is employed. The code computes a fully three-dimensional flow field through any axisymmetric bladed, rotating or stationary passage. Analysis of the flow in the bladed rotor or diffuser requires only one passage to be considered. In Pushbutton CFD, planes and surfaces for the specification of boundary conditions (at inlet, outlet, rotating and stationary walls, and periodic surfaces) are recognized automatically by the code based on the CCAD geometric model. Numerical values for the boundary conditions are established from the lower level (*e.g.*, Q3D) analysis. Also, both these values and

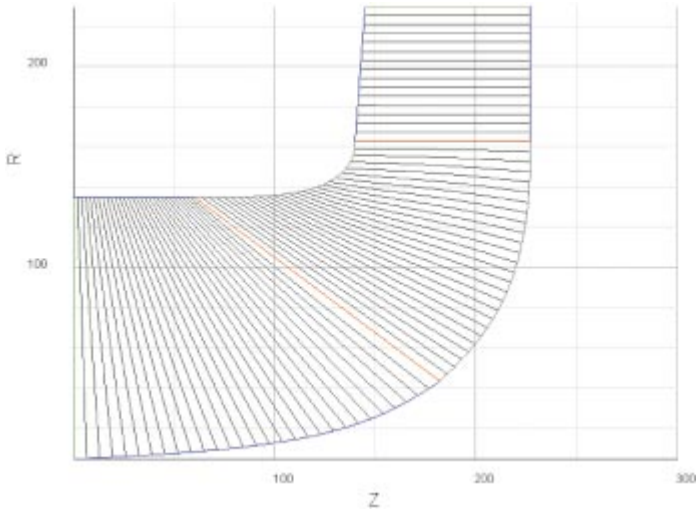

Figure 11. Impeller A 2D view of the computational domain

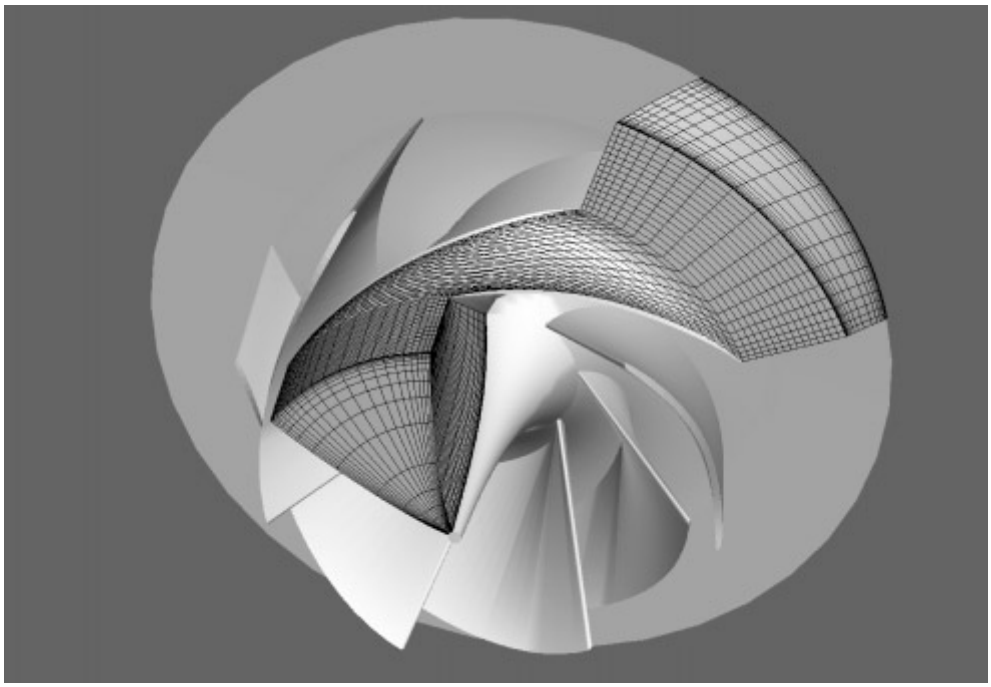

Figure 12. Impeller A 3D view of the computational domain

solver parameter settings (*i.e.*, time step multiplier, CFL, artificial viscosity coefficients, *etc.*) can be modified and adjusted by the user. At the inlet boundary condition plane, the inlet velocity vector, total pressure, and temperature are specified. At the outlet plane, the static pressure can be given and the radial variation can be computed from the simple radial equilibrium equation. The computational process, converging to a specified mass flow, can be monitored by visualizing the progress of the RMS and mass-flow errors for each iteration. Built-in criteria for the check of the convergence

terminates the process and automatically launches the graphical postprocessor. More details on the flow solver are available in [11–13].

C. Postprocessor

Two types of the postprocessor facilities are available in Pushbutton CFD and were used in this study:

- The tabulated format of the mass-and area-averaged quantities, which can be computed at an arbitrary streamwise location, and
- The graphical output of the computed quantities which can be displayed at any location of the computational planes in the 2D and 3D views, the latter with or without images of the blades or and/or grid lines.

A variety of flow and performance parameters can be selected and displayed. Available parameters include velocities and pressures plotted on the surfaces, (with or without contours), and velocity vectors with their lengths and colors proportional to their magnitude. Averaged, postprocessed quantities used in this study included impeller head rise and efficiency. Examples of the postprocessing features are given in later sections.

Pushbutton CFD was developed to be a fully automatic CFD solver, integrated in CCAD, for the purpose of performing viscous flow based analyses and performance assessments for any current blading. Some features, like storage and parallel activation and post-processing of the CFD solutions, allow a quick comparison of design alternatives and the identification of flow phenomena that enhance or deteriorate performance.

7. 3D viscous flow evaluations for impeller A

Impeller A was analyzed using the Pushbutton CFD system and the results are given below. The 2D and 3D computational domains and gridding are displayed in Figures 11 and 12, respectively.

Figure 13 presents the meridional velocity vector distributions at several pitchwise locations in the hub-to-shroud plane of impeller A. Figure 13a indicates a strong cross-flow from the hub to the shroud outlet region for the pressure side of the blade. The flow tends to change direction from the cross-flow direction toward the streamwise direction in the central regions of the passage, with a small recirculation flow region being generated at the outlet already at the middle part of the passage, Figure 13b. This local backflow region extends between the mid-passage up to a distance of about 15% of the pitch measured from the blade suction side, near the shroud contour. It produces the flow distortion that results in the flow being deflected from the main stream direction in the passage. The flow tends to be transported in the hub-to-shroud direction again (*i.e.*, with a strong cross flow bias) in the regions close to the blade suction side, Figure 13c.

Figures 14a and 14b display the meridional velocity vectors and levels, respectively, in impeller A at the mid-passage location. These plots are included to provide comparisons with similar plots, presented later, for impeller B. Figure 15 shows the

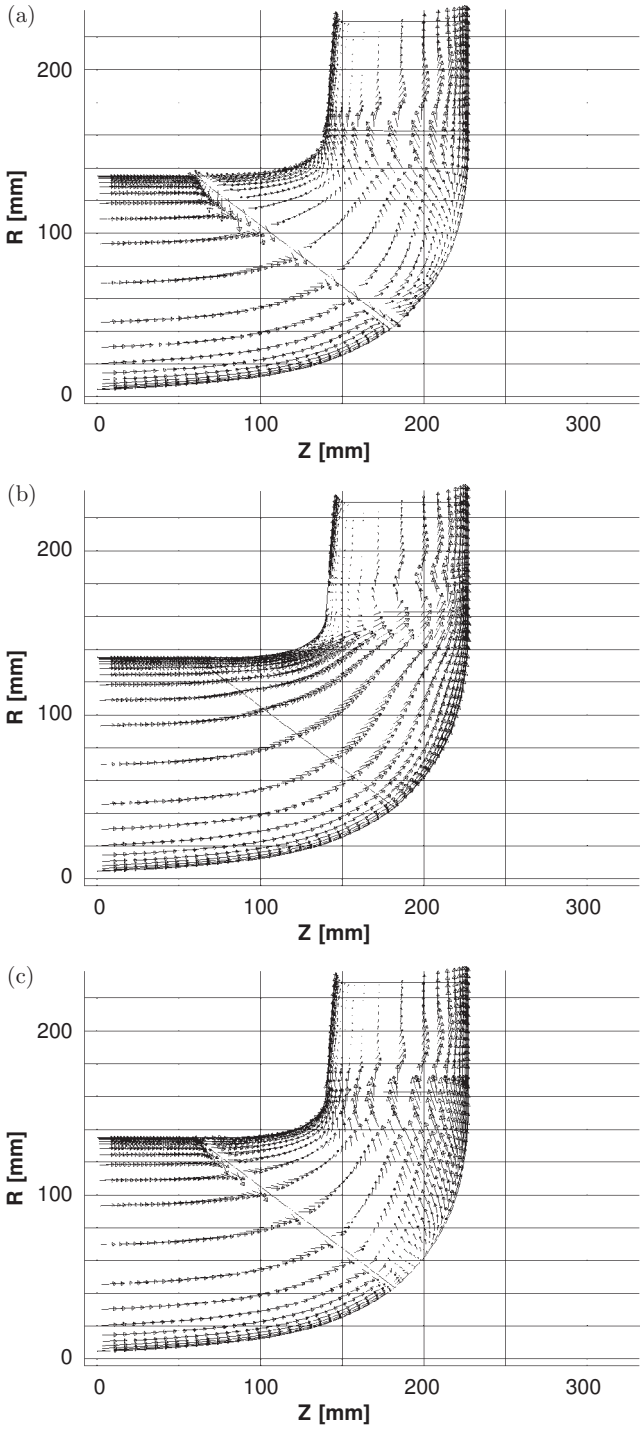

Figure 13. (a) Impeller A meridional velocity vectors close to pressure surface; (b) impeller A meridional velocity vectors near mid-passage location, closer to suction side; (c) impeller A meridional velocity vectors close to suction side

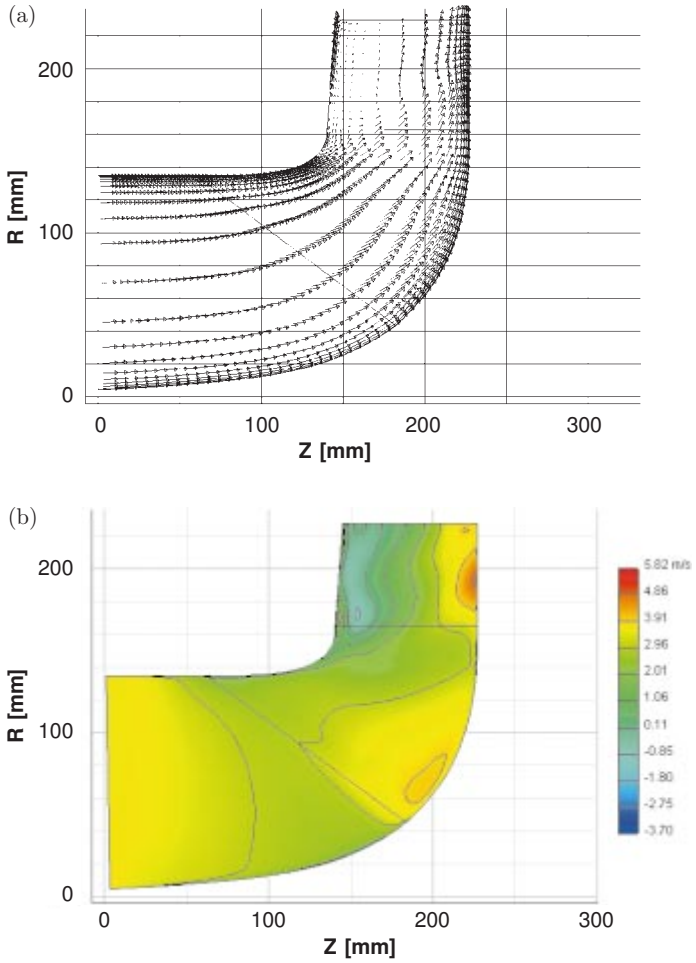

Figure 14. (a) Impeller A meridional velocity vectors at mid-passage; (b) impeller A meridional velocity distribution at mid-passage

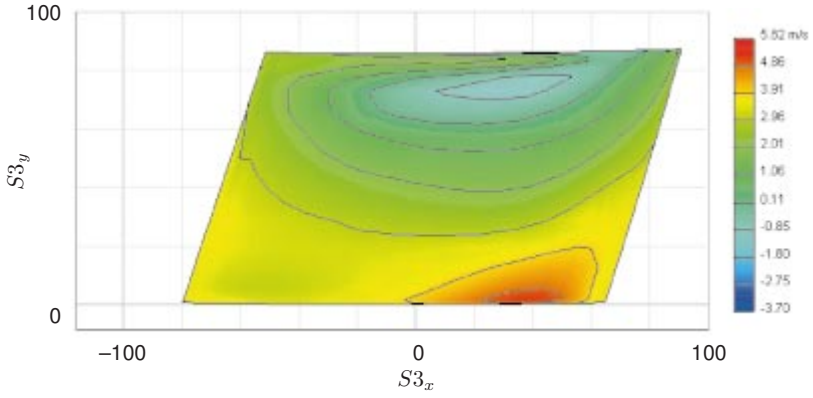

Figure 15. Impeller A meridional velocity distribution immediately after TE

velocity distribution immediately downstream of the impeller exit plane. The maximum backflow region is centered at 33% of vane pitch, with the maximum value of −1.8m/s in this region.

The Pushbutton CFD head rise prediction for impeller A is 6.83m, which is very realistic for this case as compared with the measured 5.8m for the entire pump (given the unknown spiral volute and volumetric and mechanical losses, all excluded in this analysis). These factors, when taken into account, would obviously decrease the difference between this CFD predicted value and the measured pump head of 5.8m. The CFD predicted hydraulic efficiency value for this impeller is 0.869, which is low compared to optimized impellers for this specific speed. This predicted efficiency level is considered a design reference for the development of impeller B.

8. Conclusions from impeller A flow evaluations

The three-dimensional analyses of impeller A indicated a possibility for improving the hydraulic layout of this impeller, primarily by providing better flow guidance in the passage. The purpose of the redesign effort was to increase the impeller efficiency by reducing both the hub-to-shroud cross flow, and the tendency for secondary flow generation, as well as the reduction of the backflow region at the outlet of the impeller. Design modifications to achieve these goals included:

1. The modification of impeller A's meridional contours more appropriate for its specific speed (*i.e.*, by introducing more of a mixed-flow impeller shape via changes in the positions of the LE and TE). These design modifications are aimed at reducing axial to radial turning and the associated passage curvatures in the meridional plane.
2. The redesign of the impeller blade angles to reduce excessive incidence angles along the leading edge of impeller A.
3. The redesign of the blade angle distributions between leading and trailing edges of the blade.

Experience with impeller designs within this range of specific speeds indicates a possibility for a decrease in blade number from 7 to 6, as well the reduction of the impeller inlet and exit widths. This was carried out along with a reduction of the impeller inlet diameter and an increase in impeller backsweep. These redesign steps, combined with the above mentioned three modifications, were aimed at decreasing the impeller internal losses by the reduction of the secondary flows as well as the size and the location of the wake regions in the impeller passages.

9. 1D design of impeller B

One-dimensional design of impeller B was performed in a two step process.

1. Application of the design database for initial sizing of the impeller (according to Figure 1) to reflect design features typical for an impeller of this specific speed, and
2. Application of the one-dimensional design analysis code to predict the performance of the impeller based on its inlet and outlet parameters.

Several design options, which differed in the impeller outlet width and blade outlet angle, were created and analyzed by the 1D code. The final results for the 1D

sizing of impeller B are summarized in Table 1. Table 2 contains the relevant flow parameters obtained from the meanline code analysis for pump B at the BEP. It is observed that the selection of the inlet diameter, and the outlet width was done to reduce the spanwise width of the impeller. The inlet blade angles along the repositioned LE were made to reduce the excessive incidence angles. The trailing edge position, width, and the blade outlet angle were changed, while keeping approximately the same impeller outer diameter. Prediction of the resulting wake size (low energy zone) in the impeller discharge region was reduced (from 0.426 to 0.28, as shown in Table 2). Comparing impeller B with impeller A, loss components were reduced resulting in the increase of predicted efficiency for impeller B. Impeller B was sized and designed to produce the required head rise of 5.8m, even with the blade number reduction from 7 to 6.

10. 3D viscous flow evaluations for impeller B

The digital model of impeller B was created in the three-dimensional geometry modeler (CCAD) based on the data transferred from the 1D (or meanline) model of impeller B. For the given impeller length, the shapes of hub and shroud contours as well as the blade angle distributions were iterated to satisfy various blade loading and velocity distribution criteria. The quasi-3D flow analysis tools were employed to guide the redesign process (final results not included). This process led to the configuration shown in Figure 16 and Figure 17, which show impeller B contours in the meridional plane, and its 3D digital impeller model, respectively. Comparing Figure 4 (for impeller A) and Figure 16 (for impeller B), it is clear that the reduction in meridional passage widths and the adjustment in LE and TE locations led to decreased contour curvatures, particularly for the shroud, as intended.

Similarly to the impeller A analysis, the three-dimensional viscous flow solver Pushbutton CFD (described earlier) was used to analyze impeller B candidate geometries.

The results of these calculations for the final impeller B design are displayed in Figures 18–20. These figures are similar to Figures 13–15 for impeller A. Figures 18a and 18b show the meridional velocity vector distributions between the hub and shroud of impeller B at locations close to the blade pressure side and in the mid-passage location, respectively. Comparing these results with those for impeller A (Figures 13a and 13b), a more uniform distribution of meridional velocity can be observed in the case of impeller B. The flow in the mid passage follows the impeller B channel in the streamwise direction. Flow patterns shown in Figure 18a and Figure 18c, close to the pressure and the suction sides of the blades, respectively, are typical for impellers with specific speeds similar to those for impeller A. The flow patterns are comparable to those presented by Goto [14], in which the flow in a mixed-flow impeller was investigated using the same CFD solver, BTOB3D. It is apparent from the comparisons of Figures 14a and 14b (for impeller A) and Figures 19a and 19b (for impeller B) that the meridional velocity is far more uniform for impeller B. While the impeller B flow field is more uniform, impeller A has two levels of cross-passage velocity, with high velocities close to the hub and low velocities and the beginning of backflow in the upper part of the passage and close to the shroud. The size of the

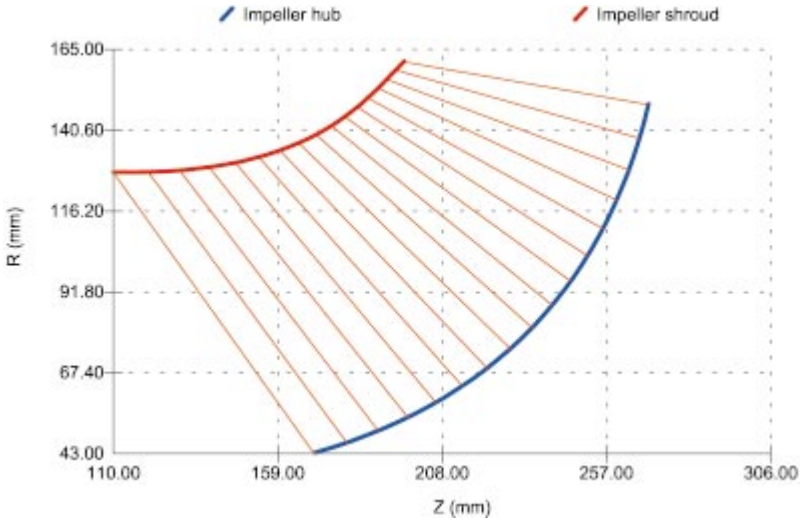

Figure 16. Meridional profile of impeller B with meshing for Q3D analysis

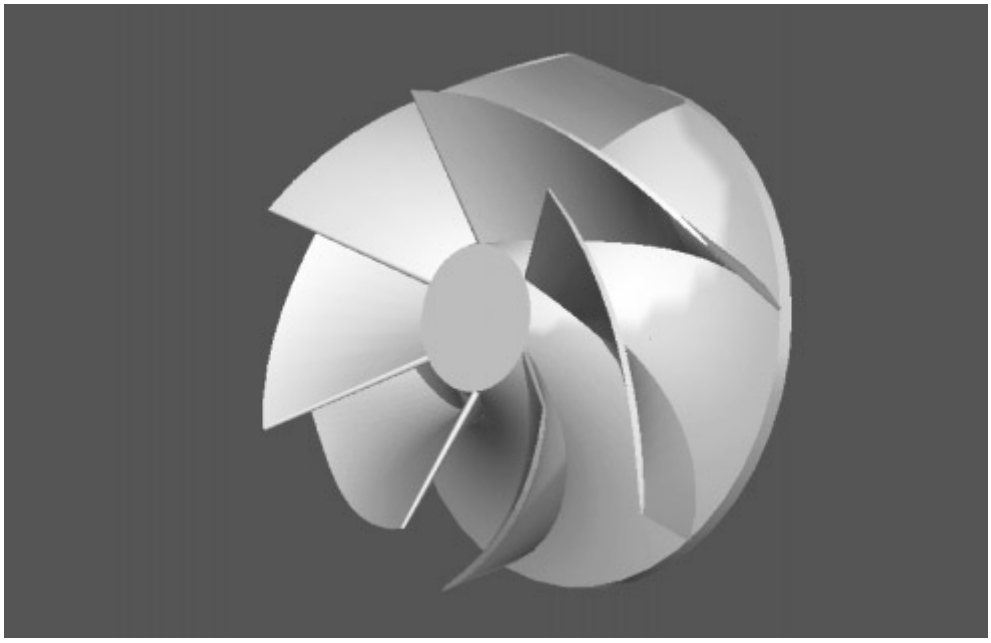

Figure 17. 3D digital impeller B model

local recirculation zone, which is created close to the impeller B shroud, is almost constant in the pitchwise direction between the mid-pitch and the suction side of the blade (see Figures 21 and 22). The blade optimization, which consisted of systematic modification and evaluation for several combinations of the shroud contour and the blade angle distribution along the shroud, resulted in the configuration in which the impeller discharge recirculation zone was moved back from the trailing edge and is located in the passage away from the impeller outlet plane. This relocation results in the decrease of the velocity gradient at the impeller B discharge plane and the

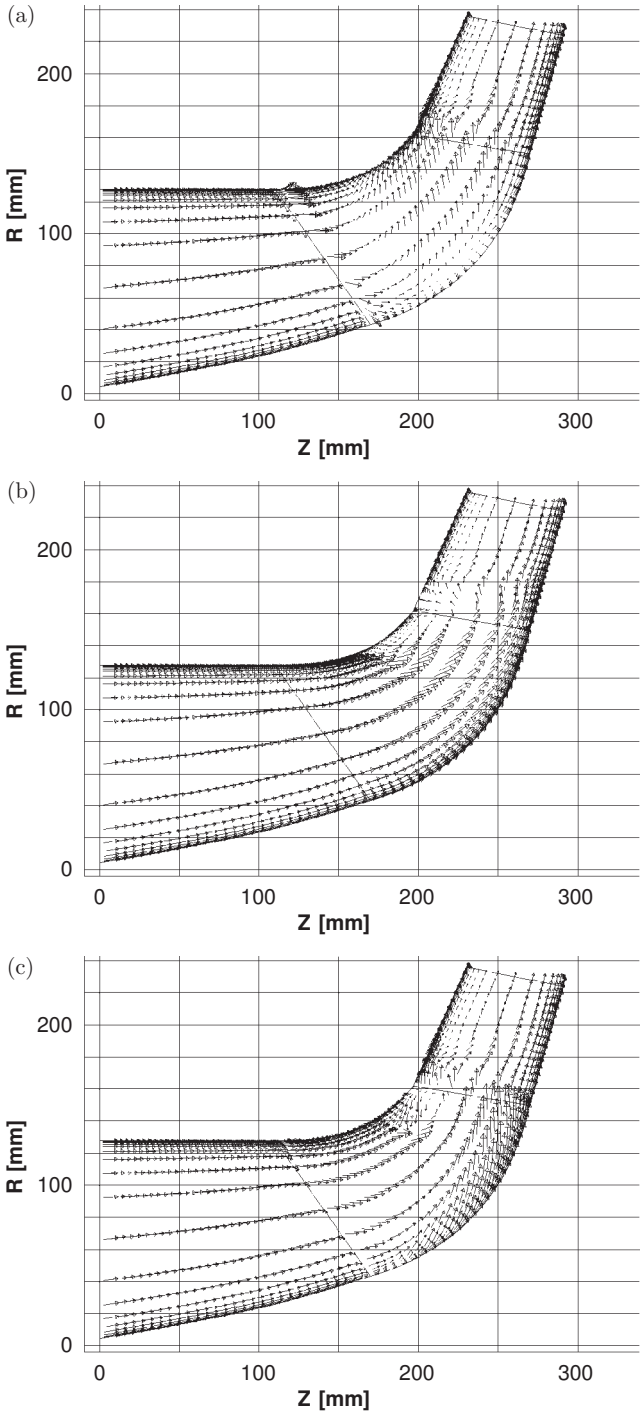

Figure 18. (a) Impeller B meridional velocity vectors close to pressure surface; (b) impeller B meridional velocity vectors near mid-passage closer to suction side; (c) impeller B meridional velocity vectors close to suction surface

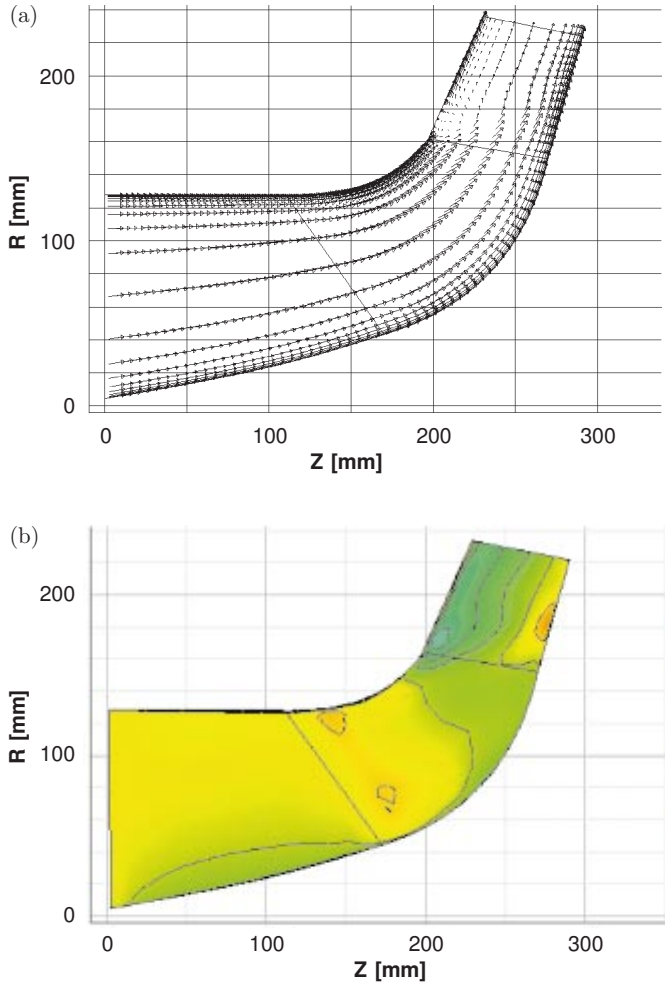

Figure 19. (a) Impeller B meridional velocity vectors at mid-passage; (b) impeller B meridional velocity distribution at mid-passage

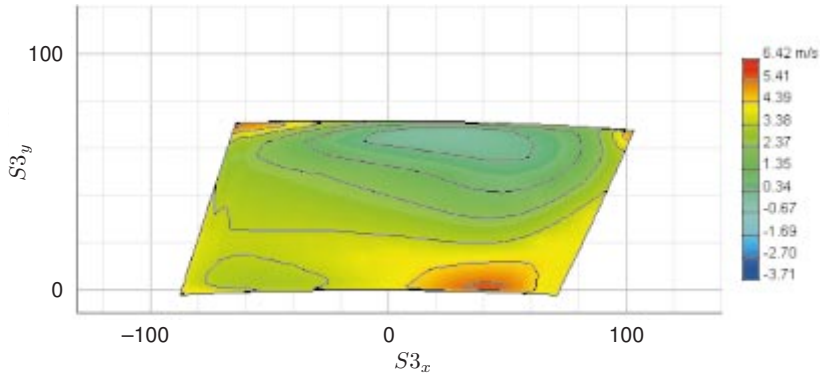

Figure 20. Impeller B meridional velocity distribution immediately after TE

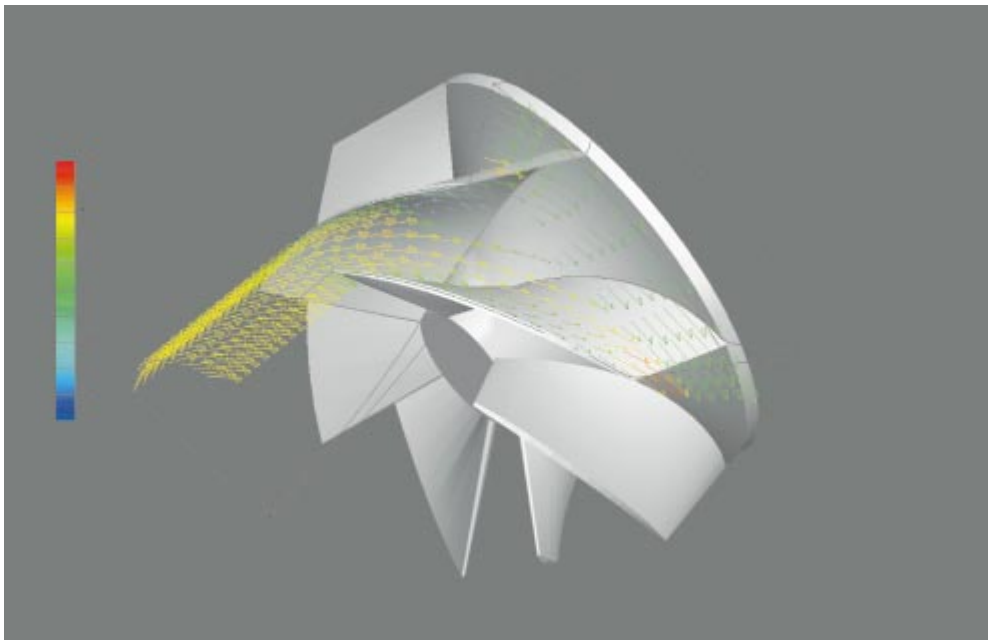

Figure 21. Location of recirculation zone behind suction side of the blade close to TE and shroud

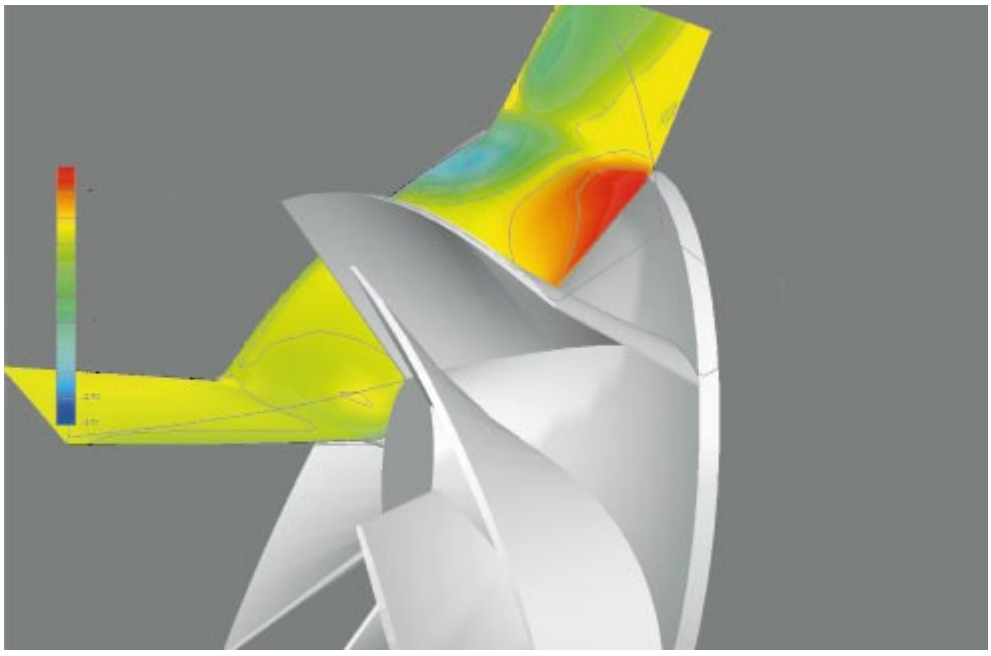

Figure 22. Location of the recirculation zone behind TE and suction side of impeller B

considerable reduction of the magnitude of the peak backflow velocity (by 66%) from $-1.8\,\mathrm{m/s}$ for impeller A to $-0.67\,\mathrm{m/s}$ for impeller B. Despite the existence of the local recirculation zone, the flow pattern across impeller B remains more uniform both in the streamwise and spanwise directions. The benefits of the performance enhancing

flow field features are confirmed by the increased efficiency, which is predicted to be 0.902 for impeller B versus 0.869 for impeller A.

11. Conclusions

The analysis of impeller A and the redesign effort for impeller B demonstrated the potential for an improvement of the existing pump impeller using the integrated modeling and flow simulation approach. The one-dimensional code was successfully applied to predict the design and off-design performance for the baseline pump with impeller A. Detailed flow analysis and generation of the impeller with improved efficiency required the combined use of the meanline code, design database for the impeller sizing, plus Q3D and fully 3D viscous flow solvers to optimize the blading. The recirculation region exists in both impellers, but differs in the size and location, being closer to the shroud/suction side corner for impeller B with a less intense and reduced region of reverse flow near the exit. The main difference between the two impellers, however, is a much more uniform flow pattern in impeller B, both in the streamwise and spanwise direction, and a considerable reduction of the cross flow in the hub-to-tip direction. This reduction of the flow transport in the direction quasi-perpendicular to the mainstream direction results in the improvement in predicted efficiency for impeller B versus impeller A (from 0.869 to 0.902).

Further work in this project will include off-design performance analyses. The detailed study will include impeller-volute interaction and will require unsteady flow computations. This work is progressing and it will be reported separately.

References

[1] Japikse D, Marscher W D and Furst R B 1997 *Centrifugal Pump Design and Performance* Concepts ETI Inc.
[2] Kaupert K 1997 *Unsteady Flow Fields in a High Specific Speed Centrifugal Pump*, PhD Dissertation, ETH-Zürich
[3] Japikse D 1987 *ASME J. Turbomachinery* **109** 1
[4] Japikse D 1991 *Proc. Int. Symp. SYMKOM*, Lodz, Poland, pp. 75–107
[5] Howard J H G and Osborne C 1977 *ASME J. Fluids Engineering* **99** 141
[6] Howard J H G, Osborne C and Japikse D 1994 *ASME Paper* **94-GT-148**
[7] CCAD – *User's Guide*, Concepts NREC
[8] PUMPAL – *User's Guide*, Concepts NREC
[9] Denton J 1994 *AGARD LS* **195***, Turbomachinery Design Using CFD*
[10] Miner S M 1997 *ASME Paper* **FEDSM97-3354**
[11] Dawes W 1987 *IMechE Paper* **C267/87**
[12] Dawes W 1988 *A Computer Program for the Analysis of Three-Dimensional Viscous Compressible Flow in Turbomachinery Blade Row* Whittle Laboratory, Cambridge University, UK
[13] Tsuei H H, Oliphant K and Japikse D 1999 *Proc. IMechE Symp. CFD Technical Developments and Future Trends*, London, UK
[14] Goto A 1990 *ASME Paper* **90-GT-36**